Proceedings of the ASME 2023
Summer Heat Transfer Conference
SHTC2023
July 10–12, 2023, Washington DC

SHTC2023-107451

NUMERICAL PREDICTIONS OF THE FLOW AND HEAT TRANSFER CHARACTERISTICS IN THE FILM BOILING REGIME DURING TUBE QUENCHING

Jayachandran K. Narayanan[1,*], Sonya Hylton[2], Mohammad Kassemi[2], Jason W. Hartwig[3], Jeffrey R. Mackey[4], Chirag R. Kharangate[1]

[1]Case Western Reserve University, Cleveland, OH
[2]National Center for Space Exploration Research, NASA Glenn Research Center & Case Western Reserve University, Cleveland, OH
[3]NASA Glenn Research Center, Cleveland, OH
[4]HX5, LLC, Brook Park, OH

ABSTRACT

Cryogenic fluid management plays a major role in refueling of spacecrafts while in space for NASA's future human space exploration missions. Due to the low boiling points of cryogens, storage, transport and handling of these fluids becomes difficult and may result in inefficient operation of the space propulsion systems. For refueling applications in space, the cryogenic fluids have to be transported across different locations and hence, the transfer of cryogenic fluids through pipes become critical. The cryogenic chill-down process is characterized by different regimes of flow boiling, viz., film boiling, transition boiling and nucleate boiling. The prediction of these regimes in a single CFD framework available in the literature is challenging and the present work attempts to address this challenge by initially modeling the film boiling regime accurately and to incorporate an user-defined function for transition and nucleate boiling at a later stage. Hence, the aim of the present work is to numerically model and validate the film boiling regime of the chilldown curve for liquid nitrogen experiments available in the literature. The validations are carried out at different inlet mass fluxes to have a robust simulation methodology. A dispersed mixture model is used to predict the vapor-liquid interface dynamics with the phase change phenomena modeled using the Lee model.

Keywords: cryogenic fluid management, chill-down, film boiling, mixture model, Lee model

NOMENCLATURE

Roman letters

t	Time [s]
v	Velocity vector [m/s]
p	Pressure [N/m^2]
g	Gravitational vector [m/s^2]
F	Surface force [N]
E	Total energy [J]
k	Thermal conductivity [W/mK]
$\dot{m}$	Mass flow rate [kg/s]
G	Mass flux [kg/m^{2}s]
T	Temperature [K]
r	Lee mass transfer coefficient

Greek letters

ρ	Density [kg/m^3]
α	Volume fraction
μ	Dynamic viscosity [kg/ms]
τ	Shear stress [N/m^2]

Subscripts

m	mixture
k,p,q	phase
dr	drift
eff	effective
op	operating
abs	absolute
w	wall
l	liquid
v	vapor
e	evaporation
c	condensation

Superscripts

T	transpose

1. INTRODUCTION

When a warmer transfer line comes in contact with a colder fluid close to its saturation temperature, the process that ensues is the transient quenching or chilldown process until the fluid flow can reach steady state. The flow regimes observed during this process are depicted in Fig. 1. When the near saturated fluid

*Corresponding author: jxk1376@case.edu

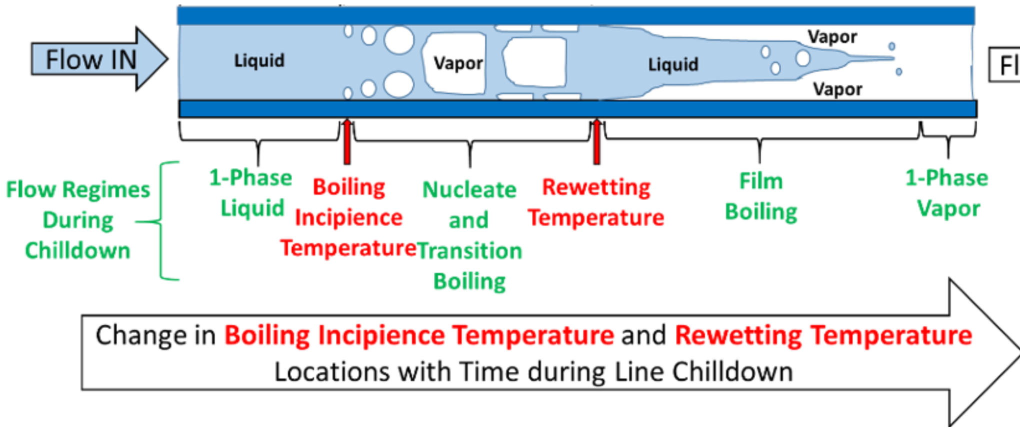

FIGURE 1: FLOW BOILING REGIMES DURING LINE CHILLDOWN PROCESS

comes in contact with the warm walls, the first step that occurs is flashing of the fluid to initiate the film boiling regime as shown in Fig. 1. In this domain, either a dispersed flow film boiling regime or the inverted annular flow film boiling regime is observed. As the chilldown process continues with no liquid to wall contact in this regime, the process will reach the Leidenfrost Point (LFP) before seeing an increase in heat flux in the transition boiling regime where the liquid starts to re-wet the heated surface. This increase in heat flux continues until the critical heat flux point (CHF) is reached, where liquid is in complete contact with the wall followed by transition to the nucleate boiling regime. The heat flux then continues to drop until all the vapor is extinguished and the single-phase forced convection domain is reached, ending the chilldown process. As observed in the flow patterns in Fig. 1, the chilldown process is accompanied by almost all the regimes of multiphase flows *viz.,* separated, mixed and dispersed flows, which makes it numerically challenging.

As discussed earlier, the chilldown process involves complex two-phase flow regimes such as dispersed, separated and mixed flows with heat transfer, phase change and fluid-solid thermal coupling. Hence, numerical/CFD modeling of the phenomena is very challenging and limited works are available in the literature. The film boiling regime which forms the first stage of the chilldown process has been modeled by some researchers due to the relatively simple stratified flow behavior at this stage [1, 2]. The CFD models that works well in the film boiling regimes starts to fail as soon as liquid starts re-wetting the wall and the flow regime transitions to nucleate boiling. Numerous works are reported in the nucleate boiling regime for refrigerants and cryogenic fluids, but are limited upto the CHF point and often fails in the film boiling regime. The reason behind this is the stratified behavior of the film boiling regimes where the interface tracking methods such as Volume of Fluid (VOF) methods work in contrast to the dispersed flow behavior in the nucleate boiling regimes where a two-fluid two-phase flow framework works better. Though the last decade saw improvements in both the methods for predictions in the other regimes, further rigorous research efforts are needed to predict a complex fluid flow and heat transfer phenomena like the chilldown process.

Kassemi *et al.* [3] has developed an in-house thoroughly validated Zero Boil-Off Tank computational fluid dynamics (ZBOT CFD) code that is based on a VOF two-phase model in the framework of ANSYS Fluent software. An important in-house customized feature of this model is accurate calculation of phase change mass transfer by performing an energy balance combined with use of the Schrage [4] kinetics relationship at the two-phase interface. The ZBOT CFD model has been validated and verified in the last ten years across different scales, fluid types, and gravitational levels through more than 30 validation case studies [3, 5]. This includes validation of its vapor-liquid interaction and phase change predictive capabilities against unique and non-intuitive microgravity data obtained by the recent ZBOT-1 ISS experiment. The ZBOT model has been successful at predicting the evaporation and condensation processes during cryogenic tank self-pressurization and subcooled jet mixing pressure control with nPFH as the working fluid in microgravity with a full 3-dimensional (3D) domain. It is currently capable of capturing the flash evaporation and simulating the resulting film boiling regime interval of the line chilldown process. To capture the nucleate and transition boiling process, the ZBOT CFD model has to be coupled to a mechanistic sub-grid model similar to the RPI boiling model promulgated by Kurul [6].

A complete line chilldown CFD model needs to have the following important inherent features in the formulation, that are not typically part of a traditional two-phase CFD code: (1) The ability to perform flash evaporation to initiate the film boiling regime, (2) A seamless and non-empirical transition between film and nucleate/transition boiling regimes, (3) The intricate mechanisms of boiling and phase change at the tube wall, and (4) The simulation of fluid flow and heat and mass transfer in the tube including the different flow boiling regimes. From the available literature, a full-CFD model that can capture the quenching curve without any thermal coupling is preferable, but not practical for this work. Initial part of the CFD validation involves capturing the film boiling regime accurately and to achieve this, the LN_2 chilldown data by Darr *et al.* [7] has been selected for comparison. Two-dimensional (2D) axi-symmetric simulations were performed using a dispersed mixture model to analyze the modeling capability in the film boiling regime. The vapor-liquid phase change dynamics has been captured using the widely used Lee phase change model. Test cases with different inlet mass fluxes were selected from the experiments to estimate the capability of the proposed modeling approach. Once the film boiling regime has been validated by the numerical framework, the methodology can be adopted to include transition and nucleate boiling regimes in the future.

2. NUMERICAL METHODOLOGY

The detailed numerical methodology has been discussed in this section including the governing equations, numerical domain and meshing, boundary and initial conditions as well as the solution methodology adopted for performing the chilldown simulations.

2.1 Governing Equations

A dispersed mixture model has been employed with the Lee phase change for predicting the boiling phenomena due to the tube quenching. The continuity equation for the mixture model is given as,

$$\frac{\partial \rho_m}{\partial t} + \nabla . (\rho_m \mathbf{v}_m) = 0 \tag{1}$$

The mass-averaged mixture velocity is calculated as,

$$\mathbf{v}_m = \frac{\sum_{k=1}^{2} \alpha_k \rho_k \mathbf{v}_m}{\sum_{k=1}^{2} \alpha_k \rho_k} \tag{2}$$

The mixture momentum equation is described as,

$$\frac{\partial}{\partial t} (\rho_m \mathbf{v}_m) + \nabla . (\rho_m \mathbf{v}_m \mathbf{v}_m) = -\nabla p + \nabla . \left[\mu_m \left(\nabla \mathbf{v}_m + \nabla {\mathbf{v}_m}^T \right) \right] + \rho_m \mathbf{g} + \mathbf{F} - \nabla . \left[\sum_{k=1}^{2} \alpha_k \rho_k \mathbf{v}_{dr,k} \mathbf{v}_{dr,k} \right] \tag{3}$$

In Eq. 3, $\mathbf{v}_{dr,k}$ is defined as the drift velocity which is computed as $\mathbf{v}_{dr,k} = \mathbf{v}_k - \mathbf{v}_m$. The surface force $\mathbf{F}$ takes account of the surface tension force which is computed by the Continuum Surface Force (CSF) model. Further, the energy equation for the mixture model is given as,

$$\frac{\partial}{\partial t} \sum_{k=1}^{2} (\alpha_k \rho_k E_k) + \nabla . \sum_{k=1}^{2} (\alpha_k \mathbf{v}_k (\rho_k E_k + p)) = \nabla . \left[k_{eff} \nabla T - (\tau_{eff} . \mathbf{v}) \right] + S_h \tag{4}$$

The volume fraction equation for the secondary phase is solved as,

$$\frac{\partial}{\partial t} (\alpha_p \rho_p) + \nabla . (\alpha_p \rho_p \mathbf{v}_m) = -\nabla . (\alpha_p \rho_p \mathbf{v}_{dr,p}) + \sum_{q=1}^{2} (\dot{m}_{qp} - \dot{m}_{pq}) \tag{5}$$

The phase change is captured using the Lee model as,

$$\dot{m}_{lv} = r_e \alpha_l \rho_l \left(\frac{T_l - T_{sat}}{T_{sat}} \right) \tag{6}$$

$$\dot{m}_{vl} = r_c \alpha_v \rho_v \left(\frac{T_{sat} - T_v}{T_{sat}} \right) \tag{7}$$

Equations 6 & 7 computes the evaporation and condensation phase change dynamics respectively with tuning of the coefficients r_e and r_c which will discussed in detail later. Finally, to capture the vapor film dynamics near the wall in the film boiling regime accurately, a SST k-ω turbulence model has been employed.

2.2 Geometry and Meshing

The numerical domain for the present CFD simulations is taken from the LN_2 chilldown experiments conducted by Darr *et al.* [7]. As the experiments were conducted in the vertical upflow configuration, a 2-D axi-symmetric numerical domain has been generated as shown in Fig. 2. The fluid domain has an inlet radius of 0.00584 m and the solid domain domain is of thickness 0.00051 m, with an overall length of 0.3456 m. Temperature measurements are available on the outer surface of the solid domain at a distance of 0.1236 m from the inlet, which will be used for validating the chilldown curves.

The fluid and solid domains are meshed as shown in Fig. 3. To clearly visulaize the grid cells, a small portion of the domain near the inlet is shown in Fig. 3. As discussed earlier, vapor films form near the wall in the film boiling regime and hence, y^+ value less than 1 is ensured at the fluid walls for capturing the film dynamics using the SST k-ω turbulence model. An element size of 0.0002 m has been used in the fluid core regions while the solid domain is divided into 10 layers in the vertical direction.

2.3 Boundary and Initial Conditions

Four test cases with different inlet mass flux have been selected from the LN_2 chilldown experiments by Darr *et al.* [7] as shown in Table 1. It should be noted that the inlet mass flux, inlet liquid temperature and operating pressure in Table 1 are averaged values over the entire chilldown period. The averaged inlet pressure from the experiments is taken as the operating pressure ($p_{abs} = p_{op} + p_{gauge}$) for defining the boundary conditions as it is not possible to define both pressure and mass flow boundary conditions at the inlet. The outlet gauge pressure is set to 0 Pa. Hence, the simulations will start with the fluid domain having absolute pressure equal to the inlet pressure and as the simulation progresses, the domain and inlet pressures change as part of the solution process. The initial wall temperature is also reported in Table 1 which will be the initial temperature condition for both fluid and solid domains. At the start of the simulation, the fluid domain is assumed to be filled with nitrogen vapor. The fluid and solid domains have a coupled thermal boundary at the walls allowing conjugate heat transfer. Vapor nitrogen is assumed as ideal gas as the density changes are significant in the operating temperature ranges of the chilldown process. The liquid nitrogen is assumed to have constant properties and SS-304 constant thermal properties has been taken for the solid domain.

2.4 Solution Methodology

An unsteady thermally coupled fluid-solid heat transfer simulation has been performed in the present study with a time step

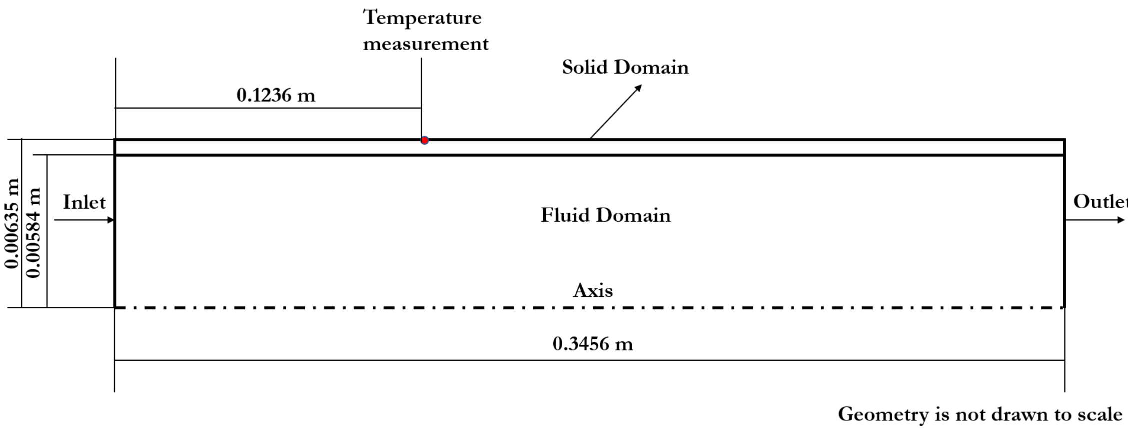

FIGURE 2: FLUID-SOLID NUMERICAL DOMAIN FROM DARR *ET AL.* [7] LN_2 CHILLDOWN EXPERIMENTS

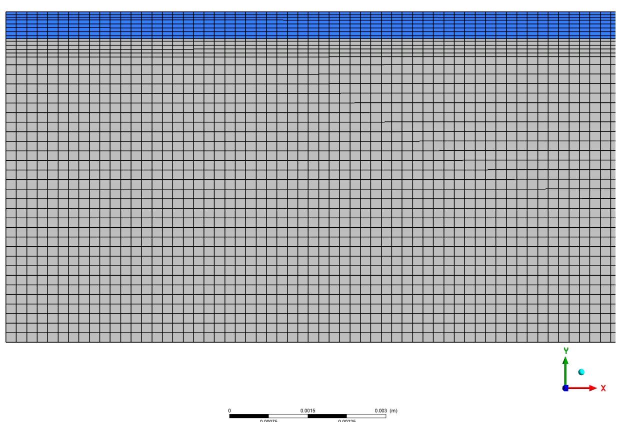

FIGURE 3: MESHING OF THE FLUID-SOLID GEOMETRY NEAR THE INLET

TABLE 1: BOUNDARY AND INITIAL CONDITIONS FOR DIFFERENT TEST CASES FROM DARR *ET AL.* [7] LN_2 CHILLDOWN EXPERIMENTS

Parameters	G [kg/m^{2}s]	T_l [K]	p_{op} [kPa]	$T_{w,initial}$ [K]
Test 1	104.31	87.23	301.70	289.23
Test 2	316.36	86.96	314.62	289.90
Test 3	788.91	85.31	490.15	290.08
Test 4	1238.54	86.68	734.62	290.38

size of 10^{-4}s. To have a reasonably converged solution, 60 iterations were carried out per time-step. For solving the two-phase flow, a dispersed mixture model has been employed. First order upwind schemes were adopted for solving the density, momentum, volume fraction, energy, turbulent kinetic energy and turbulent specific dissipation rates. For pressure-velocity coupling, a SIMPLE scheme has been selected. For unsteady terms, first order implicit transient formulation has been chosen.

3. RESULTS AND DISCUSSION

Two-dimensional axi-symmteric simulations were performed for different chilldown test cases in Table 1 and the results are discussed as follows,

3.1 Effect of Lee mass transfer coefficients

Test 2 with an inlet mass flux of 316.36 kg/m^2s has been selected to understand the effect of Lee mass transfer coefficients, *viz.*, the evaporation and condensation coefficients. For this study, both the the evaporation and condensation coefficients are kept the same value and varied in the range of 1-500 as shown in Fig. 4. The chilldown curve is obtained by plotting the variation of outer wall temperature with time at 0.1236 m from the inlet as defined by the temperature measurement location for experiments in Fig. 2. When the liquid touches the hot wall, it undergoes boiling with a rate defined by the evaporation coefficient. Higher the Lee evaporation coefficient, higher the rate of boiling and hence, the temperature drops slowly at higher Lee evaporation coefficient. This is clearly depicted in Fig. 4, where the increase in Lee coefficient shifts the chilldown curve upwards and closer to the experimental data with a good match for around Lee evaporation coefficient value of 500. In Fig. 4, only a part of the film boiling regime has been shown as the goal is to understand the effect of Lee coefficients on the chilldown curve slope in the film boiling regime while the detailed validations will be discussed in Sec. 3.2.

In the results shown in Fig. 4, though the condensation coefficient was also kept the same high value as the evaporation coefficient, it seems to have minimal effect on the slope of the chilldown curve. However, to identify whether the inference is valid for still higher Lee coefficients, simulations were performed at higher Lee coefficients upto 1500 and the results are shown in Fig. 5. It is interesting to observe that when the Lee coefficients increase above 500, the curve shifts downwards rather than shifting upwards as observed till 500. This is due to the high values of the condensation coefficients which counteract the effect of boiling due to evaporation coefficients, thus decreasing the amount of vapor generation. Though the present numerical methodology capture the film boiling regime accurately, caution should be exercised in using the solution strategy at higher Lee

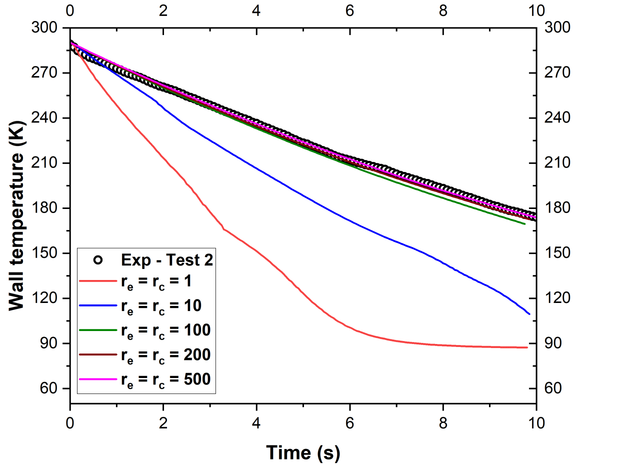

FIGURE 4: EFFECT OF LEE MASS TRANSFER COEFFICIENTS ON THE CHILLDOWN BEHAVIOR FOR TEST 2 (G = 316.36 kg/m^2s) FROM DARR *ET AL.* [7] LN_2 CHILLDOWN EXPERIMENTS

coefficients where the effect of condensation can dominate the effect of boiling.

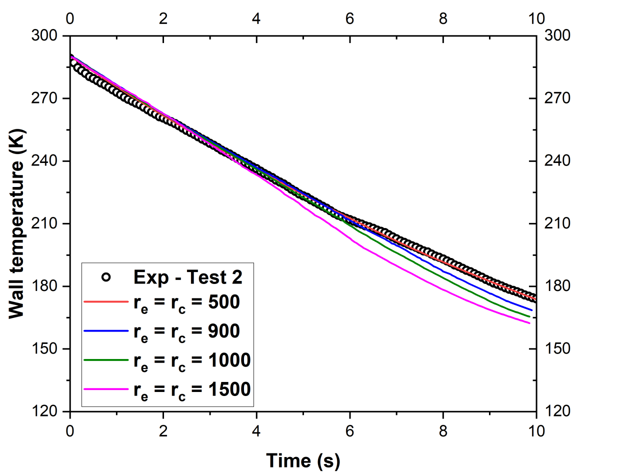

FIGURE 5: CFD PREDICTION BEHAVIOR AT HIGHER LEE MASS TRANSFER COEFFICIENTS FOR TEST 2 (G = 316.36 kg/m^2s) FROM DARR *ET AL.* [7] LN_2 CHILLDOWN EXPERIMENTS

The effect of Lee condensation coefficients at high coefficient values have been systematically explored in Fig. 6 for Test 2. As observed in Fig. 6, the Lee condensation coefficient seems to have no effect till a value of 500. At value of 1500, keeping the condensation coefficient of 0 leads to the chilldown curve shifting upward even though the curve is still below Lee coefficient value of 500 with condensation coefficient of 0. This is interesting as keeping the Lee condensation coefficient value = 0 doesn't ensure a monotonous shift of the chilldown curve upwards with increase in Lee evaporation coefficient. This points to the fact that increasing the Lee evaporation coefficient to match the experimental data should be carefully examined at higher coefficient values and there can be a limit to the test cases at low mass flow rates which can be validated with the present methodology.

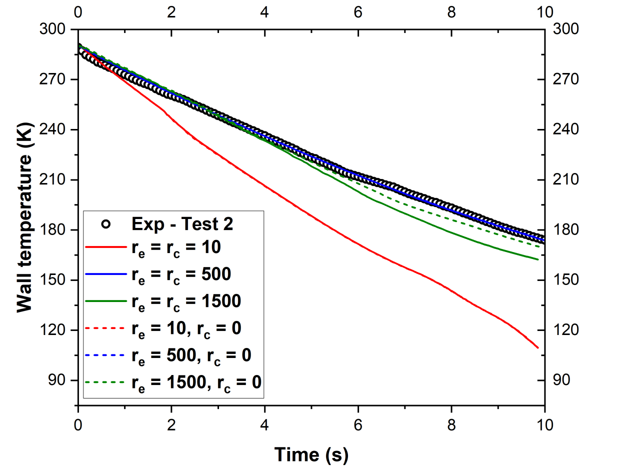

FIGURE 6: EFFECT OF LEE EVAPORATION COEFFICIENT ON THE CHILLDOWN BEHAVIOR FOR TEST 2 (G = 316.36 kg/m^2s) FROM DARR *ET AL.* [7] LN_2 CHILLDOWN EXPERIMENTS

3.2 CFD predictions at different inlet mass fluxes

The effect of Lee mass transfer coefficients for all the test cases listed in Table 1 has been performed, and an optimum Lee coefficient for each test case has been identified and reported in Fig. 7. From Fig. 7, it can be inferred that the Lee mass transfer coefficient at which the numerical chilldown curve matches experimental data decreases with increase in inlet mass flux. When the inlet mass flux increases, liquid velocities are high and cools down the pipe at a rapid rate. As a result, the amount of vapor generation will be less which agrees with the use of a lower Lee mass transfer coefficient at higher inlet mass flux. Though the present numerical methodology is not expected to perform well in the transition and nucleate boiling regimes, the simulations were continued in this regime to understand the degree of discrepancy in these regimes as in Fig. 7. Though the slope of the chilldown curve is significantly different in these regimes, a qualitative tube chilldown is still observed with the present method as the curve drops in these regions. The reasons for the drop has been explained in Sec. 3.3 with the help of liquid volume fraction and temperature distribution contours. Further, it is interesting to observe that the present methodology predicts even the transition and nucleate boiling accurately for the highest mass flow rate case. This is because the liquid moves at such a high velocity in this case that the lower Lee coefficient is enough to predict the high boiling rates in the transition and nucleate boiling regimes.

Further, in Fig. 7, at the low mass flow rate *viz.,* Test 1 (G = 104.31 kg/m^2s), keeping both the Lee mass transfer coefficients same was still under-predicting the experimental chilldown curve though the value was increased upto 1000. This is due to the condensation coefficients dominating the evaporation coefficients at high values as discussed in Sec. 3.1. Hence, further simulations were performed at very high Lee evaporation coefficients with

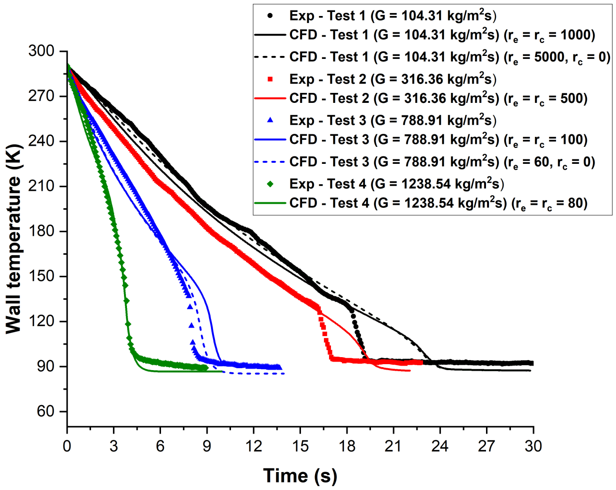

FIGURE 7: CFD PREDICTIONS AT DIFFERENT INLET MASS FLUXES FOR DARR *ET AL.* [7] LN$_2$ CHILLDOWN EXPERIMENTS

condensation coefficient set to zero and a better match in the film boiling regime was obtained at r_e = 5000. Similarly, for Test 3 (G = 788.91 kg/m^2s), the predictions are not accurate towards the end of the film boiling regime by keeping both the Lee mass transfer coefficients same. When the condensation coefficient was set to zero, a Lee evaporation coefficient of 60 predicted the results better at the end of the film boiling as well as the transition and nucleate boiling regimes.

3.3 Liquid volume fraction and temperature distributions

The liquid volume fraction and temperature contours at a section near the temperature measurement location has been plotted in Figs. 8 & 9 respectively for the validated simulation of Test 2. At the start of the simulations, the domain is completely filled with vapor at temperatures close to the initial wall temperature as seen in Figs. 8a & 9a. As the simulation progress, a thin film of vapor forms near the wall with a dispersed interface due to the dispersed mixture model formulation predicting the film boiling regime as shown in Fig. 8b. The core liquid region will have a temperature close to the inlet temperature whereas the thin vapor film will be at a higher temperature which can be clearly visualized in Fig. 9b. At this point, the solid also starts cooling down due to the heat taken away by the fluid as a consequence of boiling. Further, at t = 10 s (Figs. 8c & 9c), the thickness of the vapor film decreases and the temperature of the solid region also drops. From Figs. 8d & 9d, as the vapor film becomes thinner, the liquid slowly starts re-wetting the solid wall and then completely fills the tube. This leads to a steeper drop in the chilldown curve which mimics the transition and nucleate boiling regimes as seen in Fig. 7, without formation of bubbles.

From the liquid volume fraction and temperature contour discussions in the present section, it can be inferred that the present numerical methodology predicts the vapor film dynamics in the film boiling regime of the chilldown process. Since the present model is able to capture the re-wetting of the liquid during chilldown, the liquid volume fractions near the wall can be used as

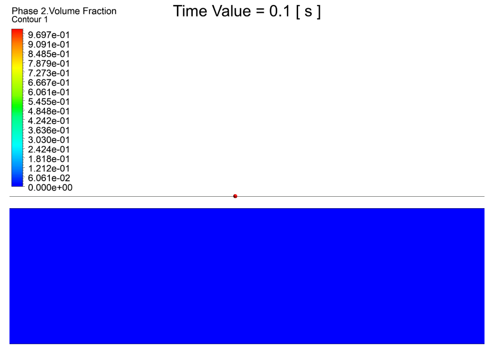

(a) Liquid volume fraction at t = 0.1 s

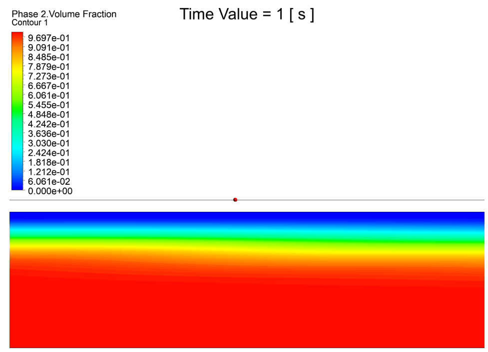

(b) Liquid volume fraction at t = 1 s

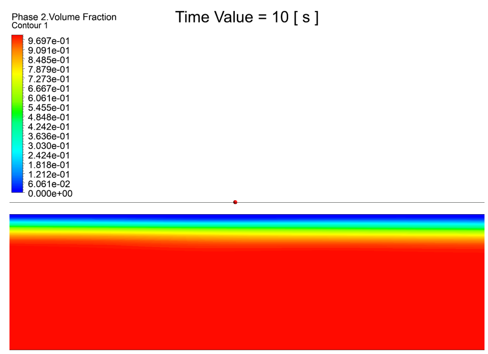

(c) Liquid volume fraction at t = 10 s

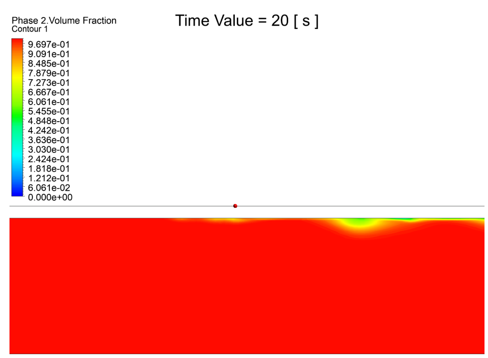

(d) Liquid volume fraction at t = 20 s

FIGURE 8: LIQUID VOLUME FRACTION PROFILES NEAR THE THERMOCOUPLE MEASUREMENT LOCATION AT DIFFERENT INSTANTS OF TIME FOR TEST 2

the starting point for the user-defined functions planned to be

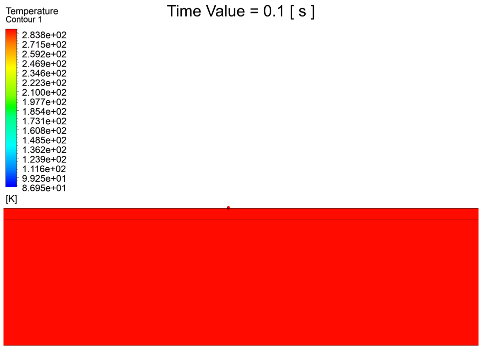

(a) Temperature profiles at t = 0.1 s

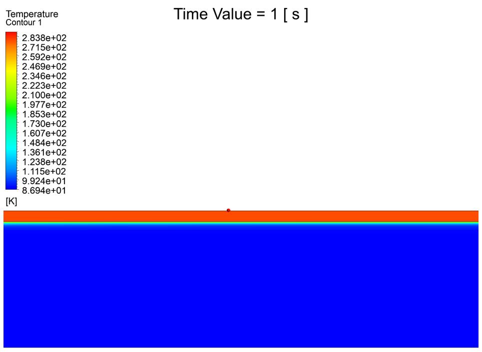

(b) Temperature profiles at t = 1 s

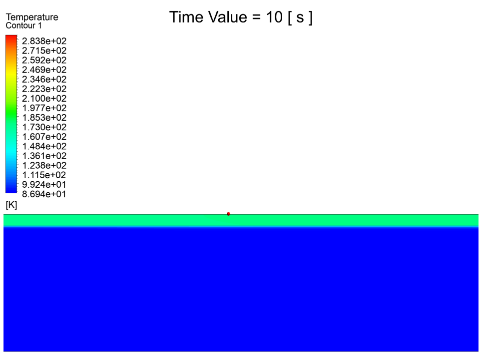

(c) Temperature profiles at t = 10 s

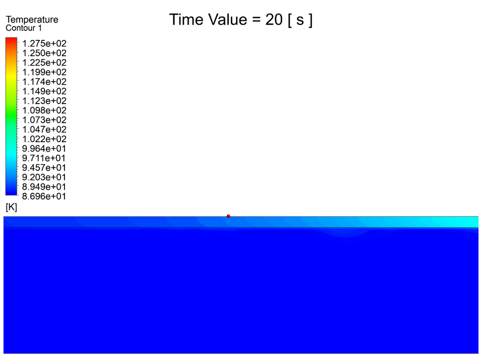

(d) Temperature profiles at t = 20 s

FIGURE 9: TEMPERATURE DISTRIBUTION PROFILES NEAR THE THERMOCOUPLE MEASUREMENT LOCATION AT DIFFERENT INSTANTS OF TIME FOR TEST 2

developed for the transition and nucleate boiling regimes. Further, 3-D simulations will be performed to analyze the robustness of the CFD methodology for flows where the effect of gravity impacts the vapor film thickness at different locations along the circumference of the tube.

4. CONCLUSION

A 2-D axi-symmetric dispersed mixture model has been employed in the present work to predict the film boiling regime of the LN_2 chilldown process. Lee phase change model seems to predict the film boiling regime to a reasonable accuracy for a wide range of inlet mass flow conditions. The effect of Lee mass transfer coefficients have been carefully examined, and it has been observed that the condensation coefficients have a significant effect at high values and needs to be set to zero for better predictions in some cases. The value of Lee evaporation coefficients for simulations which match the experimental data increases with decrease in inlet mass flux. The present approach also captures the vapor film dynamics near the wall in the film boiling regime. The model also predicts the liquid re-wetting and the drop in temperature during the transition and nucleate boiling regimes in a qualitative manner which will serve as the base for accurate modeling in these regimes in the future.

ACKNOWLEDGMENTS

The authors are grateful for the financial support of the National Aeronautics and Space Administration (NASA) under Grant no. 80NSSC22M0056. The authors also acknowledge the computational support provided by High Performance Computing (HPC) cluster at Case Western Reserve University.

REFERENCES

[1] Chen, Jianye, Zeng, Ruirui, Zhang, Xiaobin, Qiu, Limin and Xie, Junlong. "Numerical modeling of flow film boiling in cryogenic chilldown process using the AIAD framework." *International Journal of Heat and Mass Transfer* Vol. 124 (2018): pp. 269–278. DOI https://doi.org/10.1016/j.ijheatmasstransfer.2018.03.087. URL https://www.sciencedirect.com/science/article/pii/S0017931017355230.

[2] Chen, Jianye, Zeng, Ruirui, Chen, Hong and Xie, Junlong. "Effects of wall superheat and mass flux on flow film boiling in cryogenic chilldown process." *AIP Advances* Vol. 10 No. 1 (2020): p. 015123. DOI 10.1063/1.5135643. URL https://doi.org/10.1063/1.5135643.

[3] Kassemi, Mohammad, Kartuzova, Olga and Hylton, Sonya. "Validation of two-phase CFD models for propellant tank self-pressurization: Crossing fluid types, scales, and gravity levels." *Cryogenics* Vol. 89 (2018): pp. 1–15. DOI https://doi.org/10.1016/j.cryogenics.2017.10.019. URL https://www.sciencedirect.com/science/article/pii/S0011227517302576.

[4] Schrage, Robert W. *A Theoretical Study of Interphase Mass Transfer*. Columbia University Press, New York Chichester, West Sussex (1953). DOI doi:10.7312/schr90162. URL https://doi.org/10.7312/schr90162.

[5] Kassemi, Mohammad, Hylton, Sonya and Kartuzova, Olga. "1G and Microgravity Tank Self-Pressurization: Experiments and CFD Model Validations across Ra and Bo Regimes." *International Journal of Microgravity Science and Application* Vol. 37 No. 1 (2020): p. 370103. DOI 10.15011/jasma.37.1.370103.

[6] Kurul, Necdet. "Multidimensional Effects in Two-phase Flow including Phase Change." Ph.D. Thesis, Rensselaer Polytechnic Institute. 1991.

[7] Darr, S.R., Hu, Hong, Glikin, N.G., Hartwig, J.W., Majumdar, A.K., Leclair, A.C. and Chung, J.N. "An experimental study on terrestrial cryogenic transfer line chilldown I. Effect of mass flux, equilibrium quality, and inlet subcooling." *International Journal of Heat and Mass Transfer* Vol. 103 (2016): pp. 1225–1242. DOI https://doi.org/10.1016/j.ijheatmasstransfer.2016.05.019. URL https://www.sciencedirect.com/science/article/pii/S001793101630240X.